Heliyon 10 (2024) e26412

Contents lists available at ScienceDirect

Heliyon

journal homepage: www.cell.com/heliyon

Research article

Synthesis and characterization of MoS_2–COOH/gly/Mn nanocomposite as an efficient adsorbent for Ultra-trace determination of trifluralin herbicide

Kazem Karami [a,*], Ahdieh Keshmiri [a], Mohammad Reza Rezayat [a], Mohammad Taghi Jafari [a], Sedigheh Abedanzadeh [b]

[a] Department of Chemistry, Isfahan University of Technology, Isfahan, 84156-83111, Islamic Republic of Iran
[b] Department of Chemistry, Kharazmi University, Tehran, 15719-14911, Islamic Republic of Iran

ARTICLE INFO

Keywords:
Nanocomposite
Molybdenum disulfide
Extraction
Trifluralin
Herbicide
Ion mobility spectrometry

ABSTRACT

The world is confronting a severe water crisis. To clean up water from heavy metals, microorganisms, chemicals, and other types of pollutants, nanocomposites have been receiving great attention specifically due to the high surface area affording to work effectually even at low concentrations. In this research, we synthesized a new amino acid-modified MoS_2 nanocomposite by chemically immobilizing Mn (II). The synthesized absorbent MoS_2–COOH/gly/Mn was identified by thermogravimetric analysis (TGA), nitrogen adsorption measurement, X-ray diffraction (XRD), analysis of energy dispersive X-ray mapping (EDAX and MAP), field emission scanning electron microscopy (FE-SEM), and Fourier Transform Infrared spectrometry (FT-IR). The nanocomposite was employed as an adsorbent through the solid phase microextraction (SPME) method while trifluralin herbicide was chosen as a model compound. For the monitoring of trifluralin molecules, we employed an ion mobility spectrometry apparatus featuring a corona discharge ionization source. The SPME method's effectiveness was examined by investigating the stirring rate and extraction time as two crucial parameters, aiming to achieve trace analysis of trifluralin. Under the optimized condition of the trifluralin extraction, the coefficient (R^2) and linear dynamic range (LDR) correlation were obtained at 0.9961 and 0.5–10 μg L^{-1}, respectively. Relative recovery values the described approach were obtained in the span of 96–97% for agricultural wastewater samples. The quantification (LOQ) and limit of detection (LOD) were calculated at 0.5 and 0.15 μg L^{-1}, respectively. The proposed nanocomposite absorbent has the capability to be applied as an efficient material for the extraction of trifluralin herbicide from different solutions.

1. Introduction

Nanocomposites are a group of nanostructures that consist of several phases having one of the phases with dimension in the nanometer range. The first phase is actually the base or matrix of the nanocomposite, which is a crystal structure and may be made of ceramic, polymer, or metal. Another phase is distributed within the first phase (base material) as reinforcements (filler materials) for

* Corresponding author.
E-mail address: Karami@cc.iut.ac.ir (K. Karami).

https://doi.org/10.1016/j.heliyon.2024.e26412
Received 11 October 2023; Received in revised form 12 February 2024; Accepted 13 February 2024
Available online 14 February 2024

special objectives such as resistance, strength, magnetic properties, electrical conductivity, etc. Diverse properties of nanocomposites include scratch resistance, a significant surface-to-volume ratio [1], and high flexibility without reducing strength, as well as favorable optical properties like transparency, which depends on the size of the particles. From the structural point of view, particles and fibers usually create strength in the base, and the polymer base can uniformly transfer to adhere the mineral materials the forces applied to the composite to the reinforcing material [2,3].

The methods for fabricating nanocomposites are determined based on the specific field. In the polymer domain, three major fabrication methods exist, including the solvent-based method, in-situ polymerization, and melt blending. In the solvent-based method, nanomaterials and polymers are dissolved in a suitable solvent and then mixed together. Subsequently, the polymer nanocomposite is obtained in the polymer matrix by evaporating the solvent. The advantages of this method include the ease of nanomaterial dispersion in the polymer matrix due to the solvent's presence, but it is a laboratory-scale method. The selection of the solvent is determined by the type of polymer and reinforcing nanomaterial. In the in-situ polymerization method, nanomaterials and monomers are mixed together, and then by adding a catalyst and applying an appropriate temperature, the monomer is converted to polymer, and nanomaterials are dispersed within it. This method is not considered an industrial process and is more suitable for polymers that do not dissolve well in a suitable solvent or lack good thermal stability. The last method is the melt blending method, which is a fully industrial process with the capability of mass production. In this simple and rapid method, the high-temperature polymer and reinforcing nanomaterial are poured into an extruder, and by applying temperature and shear stress, the polymer melts, and the nanomaterial is dispersed in it [4].

In recent studies, there has been notable progress in the development of nanocomposites serving as nano-adsorbents, garnering considerable attention due to their enhanced physicochemical stability and augmented surface area. Particularly, magnetic nanocomposites have emerged as a textural property, reusability of nano-adsorbents, contributing to the improvement of stability, and promising alternative [5]. These magnetic nanocomposites effectively segregate materials from aqueous solutions, significantly enhancing their potential for reuse and resulting in elevated adsorptive capacity [6]. Furthermore, a parallel behavior is evident when employing magnetic nanocomposites as nano-catalysts that facilitates reusability, thereby enhancing cost-effectiveness and obviating the need for subsequent procedures such as centrifugation and filtration [7].

Over the last few years, some special two-dimensional (2D) materials were investigated as heterogeneous catalysts and adsorbents [8–10], such as various self-assembled monolayer materials [11], 2D metal oxides, graphene [12], polymers [13], and many 2D transition metal dichalcogenides (TMDCs) [14–16]. Nowadays, the numerous types of polluters such as pesticides, heavy metal ions, dyes, organic compounds, and pharmaceuticals present in sewage, encouraged researchers and scientists to focus on developing new materials [17,18]. However, using nanomaterials is accompanied by several challenges including the vast outlay of construction, pretty low reusing revenue, and environmental toxicity. Thus, there is a continuing effort to exploring materials to create suitable catalysts for the treatment of water and renewable energy.

Molybdenum disulfide (MoS_2) is selected as an integrity catalyst that resolved wastewater treatment and energy efficiency. An inorganic compound like as molybdenum disulfide is the TMDS series. Dichalcogenides are compounds of chemicals including elements oxygen, sulfur, selenium, tellurium and polonium, known as a chalcogen, and a transition metal [19]. MoS_2 is a material with three layers comparable to the structure of graphene kept all together somehow in between two layers of S atoms is put a Mo layer (S–Mo–S). Between S layers of interaction is owing to forces of van der Waal, whereas Mo–S bonds are covalent [20]. The electronic, chemical, and physical properties of this composite grasped the notice of plenty of research and were found favorable substances to substitute formerly used graphene and/or semiconductor devices. The majority of characteristics of physical MoS_2 are the same as graphene, however, it has reached premier benefit owing to its good light absorption valence and low cost. 1T, 2H, and 3R are three known phases of MoS_2 [21]. MoS_2 displayed going from bulk to structure of two-dimensional (2D) with promising and optimistic quantum and electronic characteristics [22]. Owing to its special structure, MoS_2 is used as a photocatalyst [23–25], a potential electrocatalyst [26], and a heterogeneous catalyst. Altering an indirect band gap to a direct one in a thin structure can be related to its partly great band gap (~1.8 eV). Instead of graphene, which has an almost zero-band gap, this would let downscaling electronic devices [27,28].

In 1970, Karasek and Cohen introduced ion mobility spectrometry (IMS) as a monitoring technique based on the determination of the electrophoretic mobility of the gaseous ion molecules [29]. In IMS, the ion-molecules are formed in an ionization region and moved into the drift tube and then separated by an electric field (about 300–600 Vcm^{-1}) in a drift tube and detected. The IMS application is wide such as analysis of clinical and illegal drugs, explosives, pesticides, herbicides, insecticides compounds, and environmental pollution [30].

In the current research, SPME method was performed to examine the capability of the newly synthesized nanocomposites as a proficient material for the purpose of adsorption of trifluralin herbicide from water-based samples. In this regard, IMS as a responsive apparatus for the purpose of determination of trifluralin molecules was utilized. Some of the influential parameters were fine-tuned for the extraction of trifluralin. Finally, the performance of the synthesized nanocomposite as an extraction phase was assessed in the agricultural wastewater.

2. Experimental

2.1. Materials

Trifluralin herbicide 99.0% was prepared from Kavosh Kimia Kerman Co., Iran. Deionized water, sodium molybdate 99.0% ($Na_2MoO_4.2H_2O$), monochloroacetic acid 99.0% ($ClCH_2CO_2H$), hydrochloric acid 37.0% (HCl), potassium thiocyanate 99.0% (KSCN),

sodium hydroxide 98.0% (NaOH), manganese chloride 99.0% ($MnCl_2.2H_2O$), glycine 99.0% ($C2H_5NO_2$), ethanol 96.8% (CH_3CH_2OH), and methanol 99.8% (CH_2OH) were all supplied by Merck Co.

2.2. Instrumentations

Ion mobility spectrometry instrument with corona discharge ionization source (CD-IMS) was manufactured at Teif Azmon Espadana Company. The CD-IMS details were presented in the previous works [31,32]. The synthesized manganese nanocomposite was characterized by powder X-ray diffraction (XRD, PW1730 Philips, Netherlands) along with the energy dispersive X-ray analysis (EDAX) using FE-SEM TESCAN MIRA3, Czech apparatus. A Fourier Transform Infrared spectrometer (FT-IR, Jasco-680 FT-IR Japan) was used to record FT-IR spectra. Field emission scanning electron microscopy was used by FE-SEM TESCAN MIRA3, Czech apparatus to verify the particle size of the samples and the surface morphology. Thermal characterization was carried out using TG-Q600, America at a heating rate of 10 °C.min^{-1} under argon atmosphere. Pore size and surface area were determined through the Brunauer-Emmett-Teller (BET) method by BELSORP MINI II, Japan analyzer.

2.2. Synthesis of MoS_2

The synthesis of molybdenum disulfide in this study followed the procedure outlined in prior articles [33]. A solution was created through the dissolution of potassium thiocyanate (1.22 g, 0.0125 mmol) and sodium molybdate (1.21 g, 0.005 mmol) in deionized water (60.0 mL). The prepared solution was heated in an oven at 260 °C, in a 100.0 mL Teflon-lined autoclave, for 24 h. The resultant product underwent multiple washes with distilled H_2O and was subsequently dried at 40 °C for approximately one day.

2.3. Synthesis of MoS_2–COOH

Molybdenum disulfide (0.03 g), monochloroacetic acid (1.0 g), and sodium hydroxide (1.20 g) were combined in 15.0 mL of distilled H_2O. The entire solution was stirred for a few minutes, followed by 3 h of ultrasonic dispersion. The resulting precipitate was then separated and subjected to multiple washes with distilled H_2O.

2.4. Synthesis of MoS_2–COOH/gly

MoS_2–COOH (0.35 g) and glycine (0.35 g) underwent a reaction in refluxing ethanol at 70 °C for 36 h. The resultant precipitate was filtered and subsequently dried to yield MoS_2–COOH/gly.

2.5. Synthesis of MoS_2–COOH/gly/Mn

For the synthesis of final nanocomposite, MoS_2–COOH/gly (0.01 g) was dispersed into deionized H_2O (120.0 mL) for 15 min. In the next step, manganese chloride (0.04 g) and hydrochloric acid (1.76 g) were added [34]. After 1 h of dispersion, the mixture underwent stirring for one day. The resulting product was then filtered and dried at 70 °C.

2.6. Preparation of SPME fiber

Firstly, Ni–Cr wire (diameter, 200 μm; length, 2 cm) was eluted with methanol and distilled water. A physical adhesion method was applied for coating a nanocomposite powder on Ni–Cr wire. In this regard, 2 cm of wire was immersed in a silicone binder solution (10% w/v in toluene solvent) for 1 min; then, it was withdrawn and introduced into the nanocomposite powder at ambient conditions. To dry the SPME fiber from solvent and binder, the fiber was conditioned at 220 °C for 20 min under N_2 flow (200.0 mL min^{-1}). Finally, the SPME fiber was placed on the SPME holder for the extraction procedure.

2.7. Real sample preparation

Agricultural wastewater as a real sample was collected from Isfahan University of Technology farms (Isfahan, Iran). The real sample was filtered through a 20 μm cellulose filter paper (Whatman grade 41). To eliminate the matrix effect, the sample was diluted with distilled water, to the 1:10 ratio. Finally, 10 mL of the diluted sample was applied for extraction by SPME and then analysis by CD-IMS instrument.

3. Result and discussion

Fig. 1 depicts the FT-IR spectra of MoS_2, glycine, and MoS_2–COOH/gly/Mn. A characteristic band appeared in the region 3300-3500 cm^{-1} signifies the stretching vibrations of OH functional groups. The characteristic stretching vibrations of C–H bonds with sp^3 hybrid can be observed in 2800–3100 cm^{-1} region. MoS_2–COOH exhibits S–O vibration bands at 1125 and 750 cm^{-1}, in agreement with previous published reports [35]. The FT-IR spectrum reveals a strong band at about 1740 cm^{-1} related to the carboxylate groups. Bands at 1450 and 1375 cm^{-1} are regarded to the bending vibrations of C–H bonds with sp^3 hybrid. The robust band at around 950 cm^{-1} suggests the establishment of the Mo–S bond. In the final nanocomposite, the heightened intensity of the band located at 600

cm^{-1} confirms the incorporation of Mn metal into the main structure.

Fig. 2 displays the XRD patterns of MoS_2 and the final nanocomposite. Characteristic peaks for MoS_2 at 14.39°, 39.54°, and 49.78° correspond to the (002), (103), and (105) planes, respectively, aligning with the standard card ID JPCDS 006-0097-0097. Notably, the XRD pattern of final nanocomposite closely mirrors that of pure MoS_2 in the 2θ range of 10°–25°, indicating the preservation of the MoS_2 structure in the nanocomposite.

In Fig. 3 (A and B), FE-SEM images depict the nanocomposite formed as stacked sheets, with the histogram illustrating the thickness distribution of the plates. The average thickness, calculated as 52 nm using Digimizer software, indicates the preserved structure of the nanoplates uniformly dispersed on the MoS2 sheet surface. Fig. 3C presents a TEM image in accordance with the shape and size detected in FE-SEM images for the final nanocomposite.

The EDAX analysis confirmed the existence of the Mo, S, C, O, N, and Mn elements in final nanocomposite (Fig. 4a). The elemental mapping was employed to confirm the distribution of the elements (Fig. 4b).

In Fig. 5, the thermal stability of MoS_2, MoS_2–COOH, MoS_2–COOH/gly, and final nanocomposite was assessed through thermogravimetric analysis (TGA) [36]. Fig. 5a illustrates several-step weight losses for MoS_2 nanocomposite [35]. Around 100 °C, a primary mass loss occurs due to the evaporation of adsorbed water molecules. Another weight loss at approximately 300 °C is ascribed to sulfur from the breakdown substance (MoS_2 oxidized to MoO_3), remaining stable up to 800 °C [37]. For MoS_2–COOH and MoS_2–COOH/gly substances (Fig. 5b and c), the primary mass reduction occurs around 200 °C, associated with the elimination of adsorbed water and thermal breakdown of containing oxygen groups. This results in the decomposition of CO, CO_2, and, ultimately, glycine and COOH in the range of 450–800 °C [38]. Fig. 5d displays the TGA graphs of final nanocomposite, with the primary mass loss at around 100 °C caused by the evaporation of water undergoing adsorption. The following reduction mass between 100 and 350 °C is related to the removal of carboxyl groups attached to the nanocomposite's surface. The third step beyond 350 °C involves the breakdown of organic components within the composite structure. The observed intermolecular binding among functional groups located onto the surface of material contributes significantly to the enhanced thermal durability of the nanocomposite.

Fig. 6 displays the N_2 desorption/adsorption isotherm of the final nanocomposite using the BET method. The calculated area on the surface for the final nanocomposite is 7.47 m^2/g. The results reveal type-II curves with H_3 hysteresis loops. Additionally, the mean pore size and total pore volume are determined as 29.077 nm and 0.054 cm^3g^{-1}, respectively.

3.1. Investigation of some parameters of the SPME technique

To increase the trifluralin extraction by the proposed method, some important parameters containing the stirring rate of the aqueous solution and extraction time were selected and optimized.

3.2. Stirring rate

Sample agitation is the main parameter for trifluralin extraction that is associated with the mass transfer process between the sample solution and the adsorbent phase, diminishing the thermodynamic equilibrium time [39]. To check the parameter on the

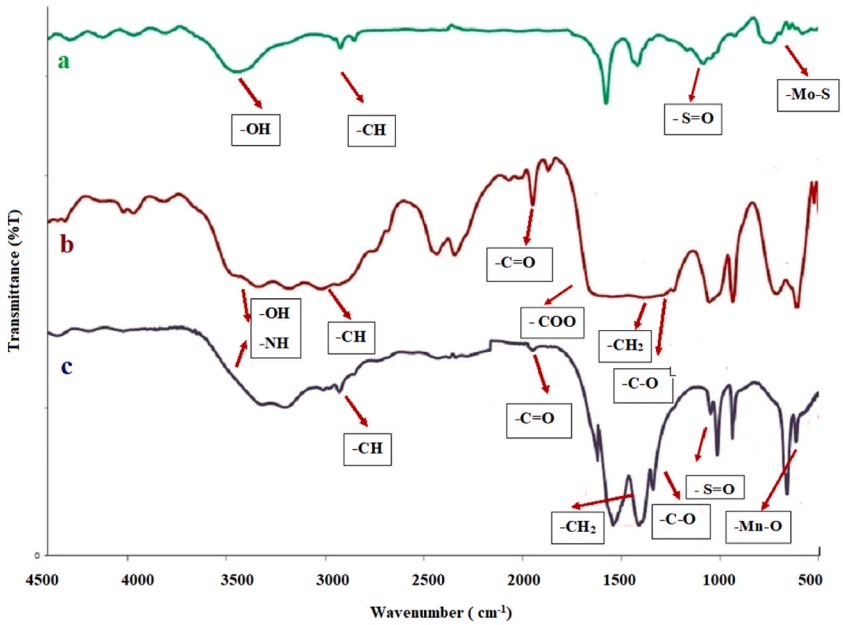

Fig. 1. FT-IR spectra of a) MoS_2, b) glycine, c) MoS_2–COOH/gly/Mn nanocomposite.

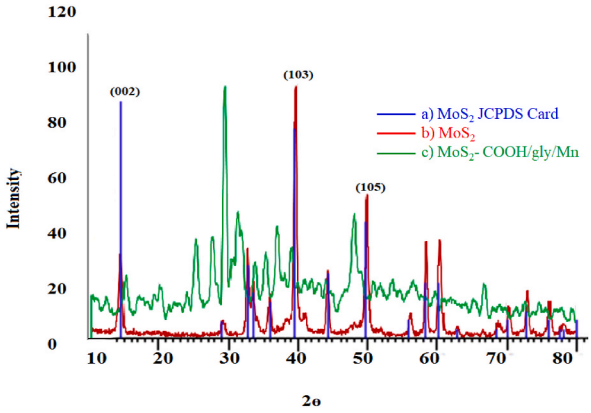

Fig. 2. XRD patterns of nanocomposite of a) MoS_2 JCPDS Crad, b) MoS_2, c) MoS_2–COOH/gly/Mn nanocomposite.

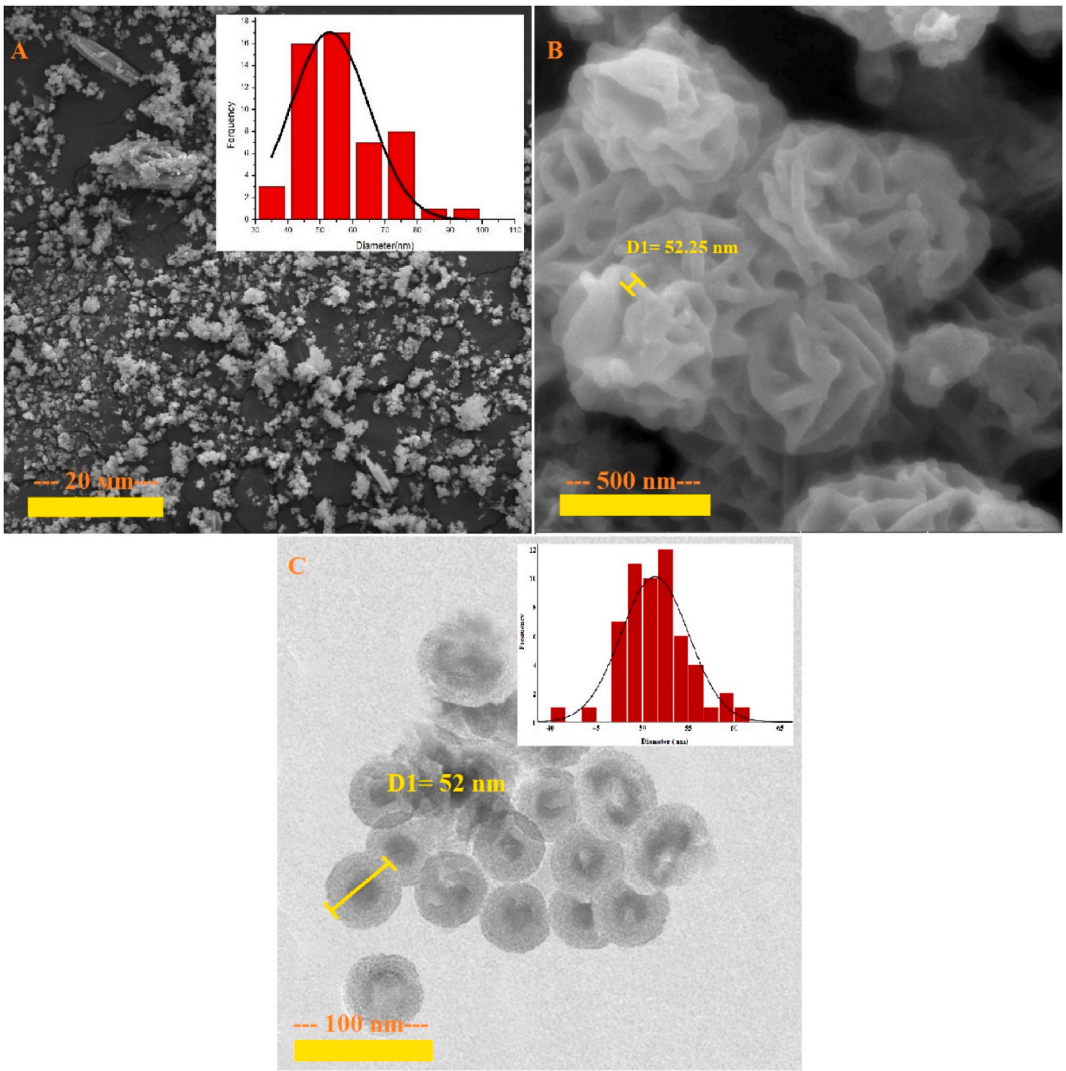

Fig. 3. A and B) FE-SEM images and C) TEM image of MoS_2–COOH/gly/Mn nanocomposite.

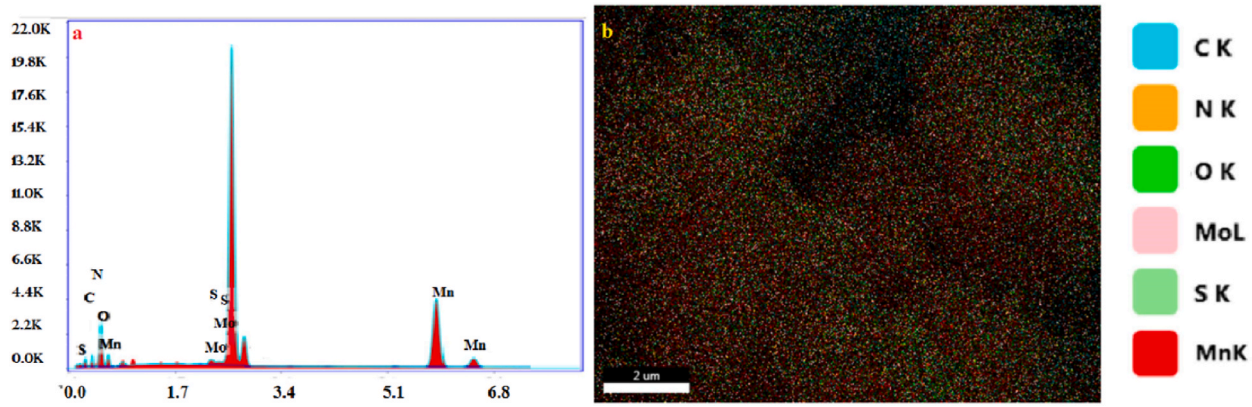

Fig. 4. (a) EDAX and (b) MAP of MoS_2–COOH/gly/Mn nanocomposite.

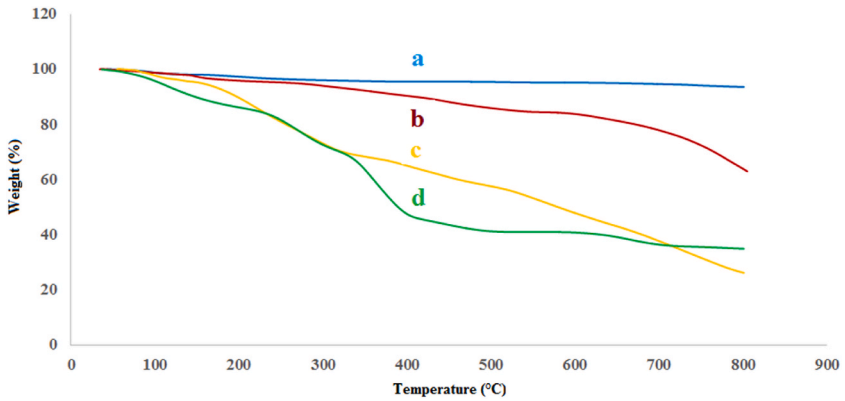

Fig. 5. TGA thermograms of (a) MoS_2, (b) MoS_2–COOH, (c) MoS_2–COOH/gly, (d) MoS_2–COOH/gly/Mn nanocomposite.

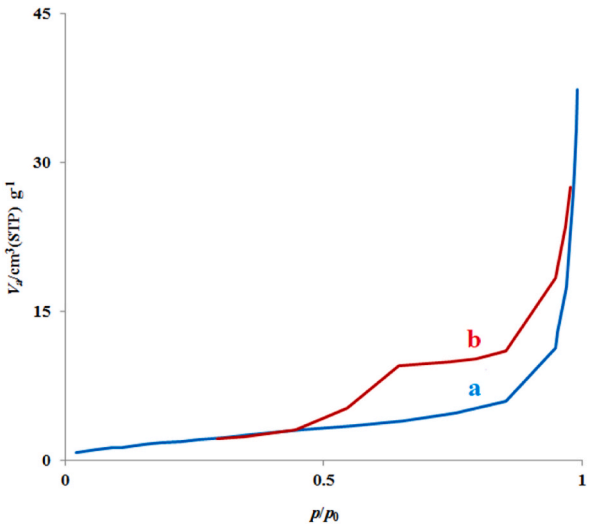

Fig. 6. BET absorption-desorption isotherm of a) adsorption, and b) desorption obtained for final nanocomposite.

trifluralin extraction, different stirring rates from 200 to 1000 rpm were chosen and optimized. According to Fig. 7, the best extraction of the analyte of the proposed method was attributed to 600 rpm.

3.3. Extraction time

In the SPME method, the extraction duration of the analyte is associated with the time of equilibrium between the trifluralin solution and SPME fiber [40,41]. To that end, different extraction times of 5–20 min were evaluated and optimized. As can be shown in Fig. 8, the equilibrium time was achieved at 10 min and selected as an optimal point.

3.4. Reusability of the SPME fiber

The chemical and mechanical stability of MoS_2–COOH/gly@Mn as SPME adsorbent are crucial parameters in practical applications. To assess the nanocomposite reusability, the extraction efficiencies were compared after 1- and 30-times extractions. After 30 extraction cycles, there was not a significant difference in the efficiency of extraction of the target analyte.

3.5. Analytical parameters

To examine the ability of the developed method with a novel adsorbent, several analytical variables containing, correlation coefficient (R^2), the limit of detection (LOD), linear dynamic range (LDR), and the limit of quantification (LOQ) were computed for analyzing of trifluralin herbicide by CD-IMS instrument. To that end, some concentrations of the trifluralin herbicide in the range of 0.50–20.0 μg L^{-1} were provided in the aqueous sample. Firstly, the molecules of the trifluralin were adsorbed by SPME adsorbent, and then, injected into the CD-IMS apparatus. Fig. 9 shows the proposed mechanism for the trifluralin using the MoS_2–COOH/gly@Mn. To plot the calibration curve (Fig. 10), the least square method was utilized, so, the LOQ and LOD were obtained at 0.50 and 0.15 μg L^{-1}, with the S/N = 3 and S/N = 10, respectively. The correlation coefficient value and LDR were acquired at 0.9961 and 0.50–10.0 μg L^{-1}, respectively. To determine the repeatability of the developed method, relative standard deviation (RSD%) was applied for three consecutive extractions at the trifluralin concentration of 2.0 μg L^{-1} and computed at 4%. In statistics and probability theory, the RSD as a repeatability index is a frequently used formula that generates a standardized measurement of the standard deviation to the mean ratio. In the two concentration levels of trifluralin (1 μg L^{-1} and 5 μg L^{-1}), the relative recoveries values as well as standard deviation of the described approach were obtained at 97% ± 10 and 96% ± 9 for the agricultural wastewater sample, respectively.

4. Conclusion

In this study, a simple process was introduced to synthesize a new nanocomposite modified by amino acid, based on fundamental materials via hydrothermal method. The physiochemical properties of the synthesized nanocomposite were fully identified using various techniques. The present study, represents the first attempt on the usage of the nanocomposite with excellent thermal and mechanical stability as an SPME coating. The method was used to extract of trifluralin herbicide from aqueous samples and the corona discharge-ion mobility spectrometry, as an exceptionally sensitive and rapid technique, it was employed to identify the trifluralin molecules. The relative standard deviation (n = 3) was computed at 4.0% to examine the repeatability of the developed method. To evaluate the selectivity of the recommended approach for determining different compounds by IMS apparatus, the values of drift time can be used as a separation factor in IMS. The high porosity hydrogen bonding, and electrostatic attractions between the synthesized nanocomposite and trifluralin molecules, increased the amazing extraction efficiency of trifluralin.

Data availability statement

No data was used for the research described in the article.

Contributions

Each author declares substantial contributions through the following:

(1) The conception and design of the study, or acquisition of data, or analysis and interpretation of data, (2) drafting the article or revising it critically for important intellectual content,

Please indicate for each author the author contributions in the text field below. Signatures are not required.

Kazem Karami & Mohammad Taghi Jafari & Sedigheh Abedanzadeh: Project administration, Resources, Supervision, Validation, and Funding acquisition.

Ahdieh Keshmiri & Mohammad Reza Rezayat: Methodology, Investigation, Conceptualization, Writing - original draft, Formal analysis, Writing review & editing, Methodology, Data curation, and Software.

Approval of the submitted version of the manuscript

Please check this box to confirm that all co-authors have read and approved the version of the manuscript that is submitted. Signatures are not required.

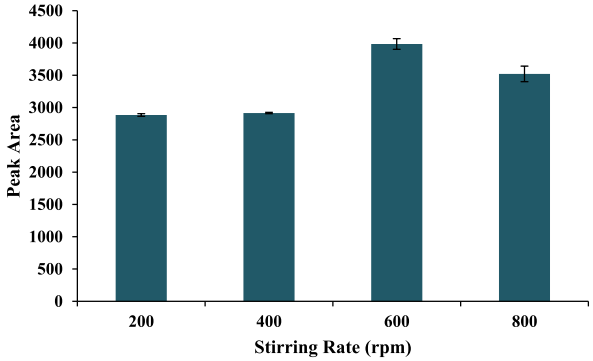

Fig. 7. The effect of sample agitation on the trifluralin extraction.

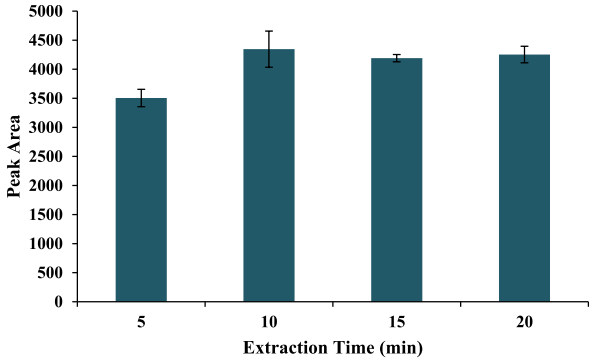

Fig. 8. The effect of extraction duration on the trifluralin extraction.

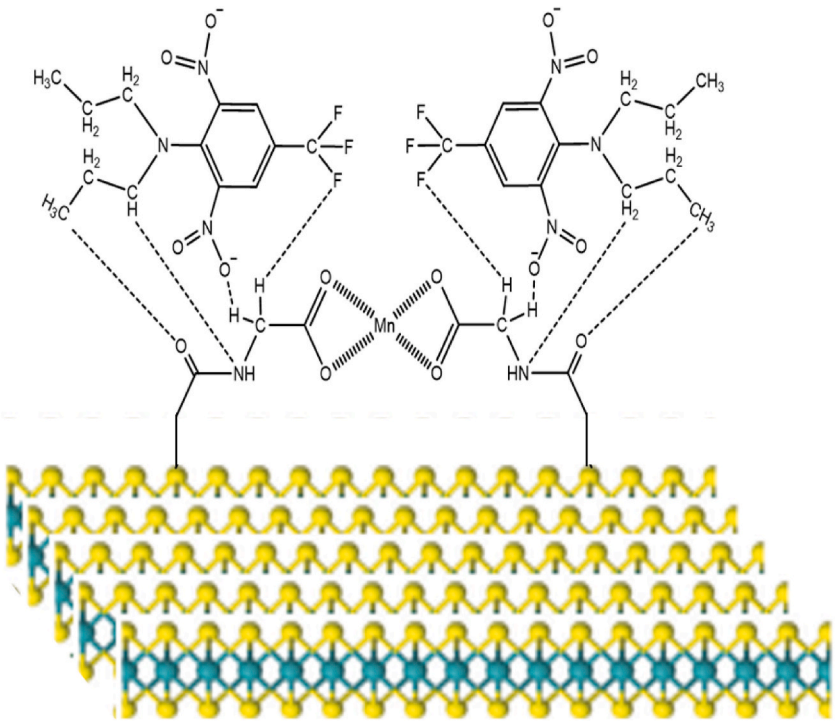

Fig. 9. Proposed mechanism for adsorption of trifluralin on the MoS_2–COOH/gly/Mn nanocomposite.

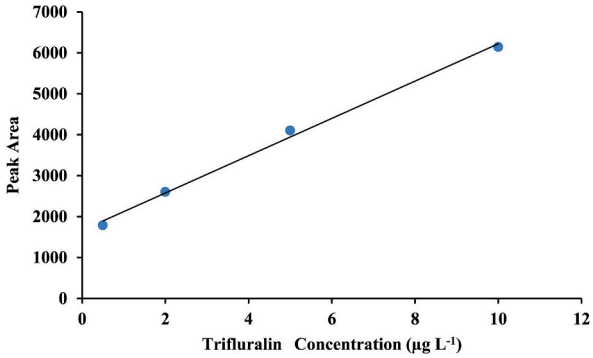

Fig. 10. The calibration curve of the proposed approach.

CRediT authorship contribution statement

Kazem Karami: Validation, Resources, Project administration, Funding acquisition. **Ahdieh Keshmiri:** Writing – review & editing, Writing – original draft, Software, Methodology, Investigation, Formal analysis, Data curation, Conceptualization. **Mohammad Reza Rezayat:** Writing – review & editing, Writing – original draft, Software, Methodology, Investigation, Formal analysis, Data curation, Conceptualization. **Mohammad Taghi Jafari:** Validation, Supervision, Resources, Project administration, Funding acquisition. **Sedigheh Abedanzadeh:** Writing – review & editing, Validation, Resources, Project administration, Funding acquisition.

Declaration of competing interest

The authors declare that they have no known competing financial interests or personal relationships that could have appeared to influence the work reported in this paper.

As the authors of this article we hereby declare that have no financial and personal relationships with other people or organizations and there are no interests to declare. The disclosed information is correct and that no other situation of real, potential or apparent conflict of interest is known to me. We undertake to inform you of any change in these circumstances, including if an issue arises during the course of the meeting or work itself.

References

[1] C. Zhu, D. Du, A. Eychmüller, Y. Lin, Engineering Ordered and nonordered porous noble metal nanostructures: synthesis, assembly, and their applications in electrochemistry, Chem. Rev. 115 (2015).
[2] C. Li, E. Thostenson, T.-W. Chou, Sensors and actuators based on carbon nanotubes and their composites: a review, Compos. Sci. Technol. 68 (2008) 1227–1249.
[3] C. Pelin, D. Ion, A. Stefan, G. Pelin, Nanocomposites as advanced materials for aerospace industry, INCAS BULLETIN 4 (2012) 57–72.
[4] A. Shojaei, P. Nourbakhsh, M. Faghihi, An investigation on the structural characteristics and reinforcement of melt processed polyamide 66/multiwalled carbon nanotube composites, Polym. Adv. Technol. 25 (2014) 406–417.
[5] F.d.S. Bruckmann, et al., Influence of magnetite incorporation into chitosan on the adsorption of the methotrexate and in vitro cytotoxicity, Environ. Sci. Pollut. Control Ser. 29 (2022) 70413–70434.
[6] B. Rahimi, N. Jafari, A. Abdolahnejad, H. Farrokhzadeh, A. Ebrahimi, Application of efficient photocatalytic process using a novel BiVO/TiO2-NaY zeolite composite for removal of acid orange 10 dye in aqueous solutions: modeling by response surface methodology (RSM), J. Environ. Chem. Eng. 7 (2019) 103253.
[7] O. Falyouna, O. Eljamal, I. Maamoun, A. Tahara, Y. Sugihara, Magnetic zeolite synthesis for efficient removal of cesium in a lab-scale continuous treatment system, J. Colloid Interface Sci. 571 (2020) 66–79.
[8] P. Miró, M. Audiffred, T. Heine, An atlas of two-dimensional materials, Chem. Soc. Rev. 43 (2014).
[9] A. Mittal, R. Ahmad, I. Hasan, Iron oxide-impregnated dextrin nanocomposite: synthesis and its application for the biosorption of Cr(VI) ions from aqueous solution, Desalination Water Treat. 57 (2015) 1–13.
[10] R. Zhao, et al., Two-dimensional tantalum disulfide: controlling structure and properties via synthesis, 2D Mater. 5 (2017).
[11] L.M. Pandey, Surface engineering of nano-sorbents for the removal of heavy metals: interfacial aspects, J. Environ. Chem. Eng. 9 (2021) 104586.
[12] H. Zhang, Ultrathin two-dimensional nanomaterials, ACS Nano 9 (2015) 9451–9469.
[13] H. Aghamollaei, et al., in: V. Grumezescu, A.M. Grumezescu (Eds.), Materials for Biomedical Engineering, Elsevier, 2019 xvii-xxi.
[14] S.Z. Butler, et al., Progress, challenges, and opportunities in two-dimensional materials beyond graphene, ACS Nano 7 (2013) 2898–2926.
[15] G.R. Bhimanapati, et al., Recent advances in two-dimensional materials beyond graphene, ACS Nano 9 (2015) 11509–11539.
[16] H. Nazer, Y. Mohamed. (2021), pp. 173-183..
[17] H. Huang, X. Feng, C. Du, S. Wu, W. Song, Incorporated oxygen in MoS 2 ultrathin nanosheets for efficient ORR catalysis, J. Mater. Chem. A 3 (2015).
[18] A. Jawed, V. Saxena, L. Pandey, Engineered nanomaterials and their surface functionalization for the removal of heavy metals: a review, J. Water Proc. Eng. 33 (2019).
[19] Z. He, W.o.W.X. Que, Molybdenum disulfide nanomaterials: structures, properties, synthesis and recent progress on hydrogen evolution reaction, Appl. Mater. Today 3 (2016) 23–56.
[20] H. Wang, C. Zhang, F. Rana, Ultrafast dynamics of defect-assisted electron-hole recombination in monolayer MoS2, Nano Lett. 15 (2014).
[21] R.J. Toh, Z. Sofer, J. Luxa, D. Sedmidubský, M. Pumera, 3R phase of MoS2 and WS2 outperforms the corresponding 2H phase for hydrogen evolution, Chemical communications (Cambridge, England) 53 (2017).
[22] X. Guo, G. Yang, J. Zhang, X. Xu, Structural, mechanical and electronic properties of in-plane 1T/2H phase interface of MoS2 heterostructures, AIP Adv. 5 (2015) 097174.
[23] X. Zong, et al., Photocatalytic H2 evolution on CdS loaded with WS2 as cocatalyst under visible light irradiation, J. Phys. Chem. C 115 (2011).
[24] G.-y. Zhao, et al., Recent progress on irradiation-induced defect engineering of two-dimensional 2H-MoS2 few layers, Appl. Sci. 9 (2019) 678.

[25] J. Xie, et al., Defect-rich MoS2 ultrathin nanosheets with additional active edge sites for enhanced electrocatalytic hydrogen evolution, Adv. Mater. 25 (2013) 5807–5813.
[26] I. Song, C. Park, H.C. Choi, Synthesis and properties of molybdenum disulphide: from bulk to atomic layers, RSC Adv. 5 (2014).
[27] D. Deng, et al., Catalysis with two-dimensional materials and their heterostructures, Nat. Nanotechnol. 11 (2016) 218–230.
[28] K. Novoselov, Beyond the wonder material, Phys. World 22 (2009) 27–30.
[29] R.G. Ewing, Ion mobility spectrometry, in: Gary A. Eiceman (Ed.), (New Mexico State University, Las Cruces, NM) and Zeev Karpas (Nuclear Research Center, Beer-Sheva, Israel), second ed., CRC Press (an imprint of Taylor and Francis Group), Boca Raton, FL, 2005 xvi + 350 pp. ISBN 0-8493-2247-2. Journal of the American Chemical Society 128, 5585-5586 (2006).
[30] T.L. Mathew, P. Pownraj, S. Abdulla, B. Pullithadathil, Technologies for Clinical Diagnosis Using Expired Human Breath Analysis, 2015.
[31] M. Rezayat, M. Jafari, F. Rahmanian, Thin film nanofibers containing ZnTiO3 nanoparticles for rapid evaporation of extraction solvent: application to the preconcentration of chlorpyrifos prior to its quantification by ion mobility spectrometry, Microchim. Acta 186 (2018).
[32] M. Rezayat, M. Jafari, Organic solvent supported silica aerogel thin film microextraction: an efficient sample preparation method for ion mobility spectrometry, Microchem. J. 159 (2020).
[33] Y. Tian, Y. He, Hydrothermal synthesis of fine MoS2 crystals from Na 2MoO4 and KSCN, Chem. Lett. 32 (2003) 768–769.
[34] C.-J. Wang, P.-S. Hung, S.-C. Chou, W.-A. Chung, P.-W. Wu, Synthesis of polystyrene@polypyrrole-COOH@Ag (core@shell@shell) microspheres for potential application in anisotropic conductive paste, Mater. Lett. 263 (2020) 127239.
[35] A. Bahuguna, et al., Nanocomposite of MoS2-RGO as facile, heterogeneous, recyclable, and highly efficient green catalyst for one-pot synthesis of indole alkaloids, ACS Sustain. Chem. Eng. 5 (2017).
[36] K. Karami, A. Keshmiri, S. Abedanzadeh, Selective separation of methylene blue from aqueous solution using Mn/Pd decorated chemically modified MoS2 nanocomposites, Colloids Surf. A Physicochem. Eng. Asp. 683 (2024) 133106.
[37] U.C.J.R. Jaleel, K.R.S. Devi, R. Madhushree, D. Pinheiro, Statistical and experimental studies of MoS2/g-C3N4/TiO2: a ternary Z-scheme hybrid composite, J. Mater. Sci. 56 (2021) 6922–6944.
[38] S. Stankovich, et al., Synthesis of graphene-based nanosheets via chemical reduction of exfoliated graphite oxide, Carbon 45 (2007) 1558–1565.
[39] W.A. Wan Ibrahim, H. Farhani, M.M. Sanagi, H.Y. Aboul-Enein, Solid phase microextraction using new sol–gel hybrid polydimethylsiloxane-2-hydroxymethyl-18-crown-6-coated fiber for determination of organophosphorous pesticides, J. Chromatogr. A 1217 (2010) 4890–4897.
[40] A. Kumar, Gaurav, A.K. Malik, D.K. Tewary, B. Singh, A review on development of solid phase microextraction fibers by sol–gel methods and their applications, Anal. Chim. Acta 610 (2008) 1–14.
[41] K. Karami, A. Mardaniboldaji, M. Rezayat, P. Bayat, M. Jafari, Novel UiOêÄ¸66êÄ¸NH2/gly/GO nanocomposite adsorbent for UltraêÄ¸trace analyzing of chlorpyrifos pesticide by ion mobility spectrometry, ChemistrySelect 6 (2021) 3370–3377.